


***Ab initio* simulations of x-ray emission spectroscopy with the GW+Bethe-Salpeter equation method**Tsubasa Aoki and Kaoru Ohno <sup>\*</sup>*Department of Physics, Yokohama National University, 79-5 Tokiwadai, Hodogaya-ku, Yokohama 240-8501, Japan*

(Received 10 June 2019; published 26 August 2019)

In order to calculate x-ray emission spectroscopy (XES) spectra, we apply the GW+Bethe-Salpeter equation (GW + BSE) method on a basis of extended quasiparticle theory, which enables one to treat an arbitrary excited state as an initial state, because the initial state in the XES process is a highly excited state with a core hole. Compared to the preexisting experimental data of XES fluorescence photon energy, the calculated GW + BSE results give values with about 1-eV accuracy, which is comparable to the previous results using the time-dependent density functional theory with the short-range corrected exchange-correlation functional, the equation of motion-coupled cluster single and double, and delta self-consistent field methods. Our GW + BSE results reproduce corresponding experimental XES spectra without missing any peak. The method can assign the excitonic configuration of each peak in XES spectra with the quasiparticle levels. As a result, the analysis of excitonic structure for each peak gives obvious interpretation concerning the relation between excitonic states and valence states.

DOI: [10.1103/PhysRevB.100.075149](https://doi.org/10.1103/PhysRevB.100.075149)**I. INTRODUCTION**

Recent advances in x-ray sources have led to progress in spectroscopic techniques in the x-ray region [1]. These techniques involve an excitation of a core electron, which can provide an atom specific probe of electronic structures as a powerful analytical tool used in many research fields [2,3]. As a new experimental tool, x-ray emission spectroscopy (XES) has been recognized as a useful technique for chemical analyses which give the information of valence electrons [4,5].

Theoretical calculations can play an important role in the analysis and interpretation of experimental spectra. Especially, *ab initio* calculations are becoming important tools in x-ray analysis studies [6]. Figure 1 shows the x-ray photo-processes of x-ray photoelectron spectroscopy (XPS), x-ray photoabsorption spectroscopy (XAS), and XES, respectively. While the initial state in both XPS and XAS processes is the ground state, the initial state in the XES process is the excited state with one core hole. Thus, the calculation of XES has a characteristic issue of describing the highly excited initial state which involves the screening effect with a core hole. This problem does not exist in XPS and XAS processes. It is important to perform predictive XES calculations, which match experimental spectral features and absolute energies. In recent years, *ab initio* calculation methods for the XES process have been developed [7–13].

Here, we will shortly review the previous studies of *ab initio* calculations related to the x-ray photoanalysis. Bagus showed the pioneering simulation of the XPS process by the Hartree-Fock (HF) method, which introduced the electronic relaxation of the molecular systems with a core hole [14]. This approach is now called the delta self-consistent field

( $\Delta$ SCF) method [15]. Using the  $\Delta$ SCF(HF) method, Ågren and Nordgren studied the XES spectra for the first time [16]. In order to obtain the transition energies and the intensities of XES spectra, Besley and Asmuruf [9] applied  $\Delta$ SCF(B3LYP), time-dependent density functional theory (TD-DFT) [17], and equation of motion-coupled cluster single and double (EOM-CCSD) [18] methods, which enable one to calculate XES spectra in an analogous approach of calculating XAS spectra. With respect to the x-ray fluorescence photon energies, the TD-DFT results with BLYP [19–21] and B3LYP [20,22,23] exchange-correlation functionals showed large deviations from the experimental data. The EOM-CCSD and the  $\Delta$ SCF(B3LYP) results gave good agreements with the experimental data, but there remain some problems about the spectral information of XES. For example, the number of peaks in XES spectra is different from the experiment in the carbon K-edge XES spectrum of the CH<sub>3</sub>OH molecule in Ref. [9]. Originally, XES was used as a technique of chemical analysis for the valence electronic structure. If there is a lack of peaks in XES spectra, it may give incorrect interpretation in chemical analysis. In order to avoid this kind of error, it may be required to treat the initial- and final-state effects of the XES process appropriately. However, the method is extremely complicated and the excited-state calculation has to be performed one by one. Moreover, the  $\Delta$ SCF method using density functional theory (DFT) [24,25] is not guaranteed for the XES process since DFT cannot be applied to the excited state having a core hole.

In these situations, an alternative method to give accurate x-ray fluorescence photon energy and to represent valence electronic structure of XES spectra is needed. The Green's-function approach in many-body perturbation theory [26] can be a solution to overcome this difficulty of the XES simulation. There are some favorable properties in many-body perturbation theory to apply for XES simulations. The first

<sup>\*</sup> ohno@ynu.ac.jp

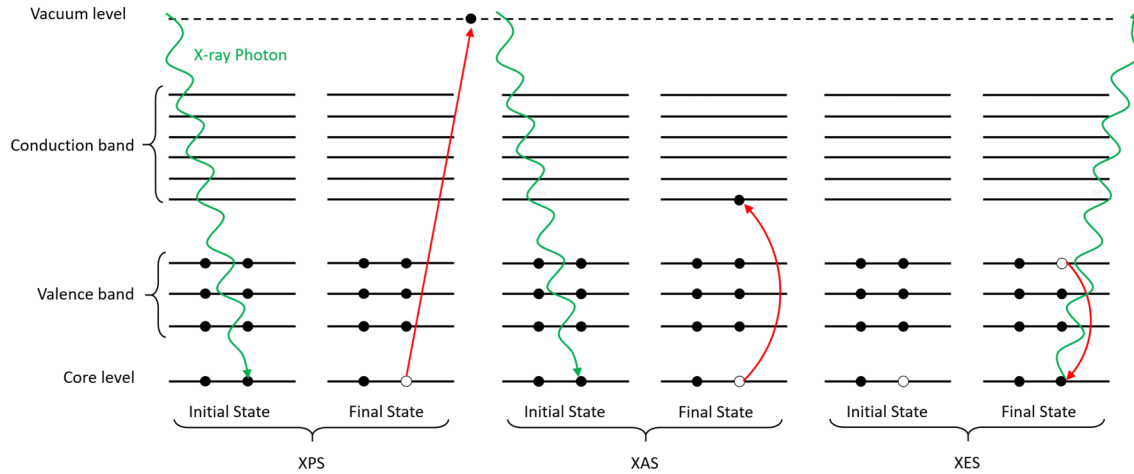


FIG. 1. Schematic image of the x-ray photoanalysis process in x-ray photoelectron spectroscopy, x-ray photoabsorption spectroscopy, and XES.

property is that the excitation spectra such as XPS, XAS, and XES can be directly treated by solving the Dyson equation or the Bethe-Salpeter equation (BSE) [27–33] in many-body perturbation theory. In fact, recent *ab initio* studies using the Green’s-function approach showed the accurate prediction of core electron binding energy in XPS simulations [34–36]. Especially, the *GW*+Bethe-Salpeter equation (*GW* + BSE) method has been widely used for simulating the XAS spectra in molecule, cluster, and solid systems [37–40]. The success of the Green’s-function approach in XPS and XAS simulations results from the accurate description of the screening effect due to the core hole state within the *GW* approximation (GWA) [41–44]. The second property is that the Green’s-function approach can treat an arbitrary excited state as an initial state, which was recently established as extended quasiparticle theory [45]. This property allows one to make the initial state with a core hole the input electronic configuration and offer a powerful justification to apply the Green’s-function method to XES simulations. There are a few XES or resonant inelastic x-ray scattering (RIXS) studies using the Green’s-function method [46–48]. However, they assume the  $N$  electron ground state as the initial state and perform a simple *GW* + BSE calculation for the valence excitation only. They treat the  $N$  electron process, not the  $N - 1$  electron process. Furthermore, they rely on some empirical parameters, which become an issue with predictive performance for XES simulations. In contrast, our initial state is the  $N - 1$  electron excited state with a deep core hole, where one electron is emitted from the core level to the vacuum level. Extended quasiparticle theory allows us to do this. Moreover, we do not use any empirical parameter at all in our calculation. In our approach, the initial state of the density functional theory *GW* + (DFT + *GW*) calculations is the core-excited system. Then we will apply the BSE, which places the excited electron into the core hole. The reader might be expecting that DFT + *GW* is for the ground state and the x-ray BSE creates a core hole. However, the opposite is true in our method. Thus, our method, using extended quasiparticle theory, is apparently different from the previous XES or RIXS studies, which start with the  $N$  electron ground state as the initial state.

There also remains a problem of basis functions to represent the wave functions of the initial state in the XES process. The electronic structure calculations in quantum chemistry usually use the Gaussian basis functions, which are not always suited to represent the excited-state wave functions with screening effect owing to its basis set incompleteness. To overcome the basis set incompleteness, we apply the all-electron mixed basis functions [49] for the quasiparticle wave functions, which have been used successfully in our previous study [34]. Using this approach, we can keep the accuracy of the *GW* + BSE method with the all-electron mixed basis functions for simulating XES spectra.

The purpose of this paper is to demonstrate that the *GW* + BSE method has enough capability to estimate accurate x-ray fluorescence photon energy in small molecular systems. Moreover, we will assign excitonic states with our calculated spectra and discuss the relationship between BSE wave functions and quasiparticle wave functions of valence electrons.

## II. METHODS

In this paper, we consistently adopt the *GW* + BSE method for XES calculations as a Green’s-function approach in an all-electron formalism. In this section, we briefly introduce the *GW* + BSE method within the Tamm-Dancoff approximation (TDA) [50] for spin-polarized systems. We use the shorthand notation  $1 = (\mathbf{r}_1, \sigma_1, t_1)$ , which stands for position, spin, and time.

Within the GWA,  $\Sigma^{GW} = iGW$ , the one-shot *GW* method [51,52] gives the quasiparticle (QP) energy  $\varepsilon^{QP}$  of a state  $(n, \sigma)$  as

$$\varepsilon_{n,\sigma}^{QP} = \varepsilon_{n,\sigma}^{KS} + Z_{n,\sigma}(n, \sigma) \left[ \left[ \Sigma_{\sigma}^{GW}(\mathbf{r}, \mathbf{r}'; \varepsilon_{n,\sigma}^{KS}) - V_{\sigma}^{KSxc}(\mathbf{r})\delta(\mathbf{r} - \mathbf{r}') \right] | n, \sigma \right], \quad (1)$$

where the renormalization factor  $Z_{n,\sigma}$  is defined as

$$Z_{n,\sigma} = \left[ 1 - \frac{\Delta \Sigma_{\sigma}^{GW}}{\Delta \varepsilon} \Big|_{\varepsilon = \varepsilon_{n,\sigma}^{KS}} \right]^{-1}. \quad (2)$$

$\varepsilon_{n,\sigma}^{KS}$ , and  $V_{\sigma}^{KSxc}$  represent the Kohn-Sham (KS) eigenvalue of a state  $(n, \sigma)$ , and the KS exchange-correlation function in

DFT, respectively [24,25]. In the one-shot *GW* method, the QP wave functions are replaced by the KS wave functions, i.e.,  $\phi_{n,\sigma}^{\text{QP}} \simeq \phi_{n,\sigma}^{\text{KS}} = |n, \sigma\rangle$ . Moreover the QP energy dependency of the self-energy within the GWA is treated by the linear extrapolation technique.

The BSE for the two-particle correlation function  $L(1, 2; 1', 2')$  is written as

$$\begin{aligned} L(1, 2; 1', 2') &= G_1(1, 2')G_1(2, 1') \\ &+ \int d(3456)G_1(1, 3)G_1(4, 1')\Xi(3, 5; 4, 6) \\ &\times L(6, 2; 5, 2'), \end{aligned} \quad (3)$$

where  $G_1$  is the one-particle Green's function and  $\Xi$  is the BSE kernel function representing the interaction between the single QPs. The BSE kernel function  $\Xi$  is given by the functional derivative as

$$\Xi(3, 5; 4, 6) = \frac{\partial \Sigma(3, 4)}{\partial G_1(6, 5)}. \quad (4)$$

$$\begin{aligned} D_{n_1, m_1; n_2, m_2}^{\sigma, \sigma'}(\Omega^\lambda) &= (\varepsilon_{n_1 \sigma}^{\text{QP}} - \varepsilon_{m_1 \sigma}^{\text{QP}})\delta_{n_1, n_2}\delta_{m_1, m_2} - \frac{i}{2\pi} \int d\mathbf{r}_1 d\mathbf{r}_2 d\omega \phi_{n_1 \sigma}^{\text{QP}*}(\mathbf{r}_1)\phi_{m_1 \sigma}^{\text{QP}}(\mathbf{r}_1)W(\mathbf{r}_1, \mathbf{r}_2, \omega)\phi_{n_2 \sigma}^{\text{QP}}(\mathbf{r}_2)\phi_{m_2 \sigma}^{\text{QP}*}(\mathbf{r}_2) \\ &\times \left[ \frac{1}{\Omega^\lambda - \omega - (\varepsilon_{n_2 \sigma}^{\text{QP}} - \varepsilon_{m_1 \sigma}^{\text{QP}})} + \frac{1}{\Omega^\lambda + \omega - (\varepsilon_{n_1 \sigma}^{\text{QP}} - \varepsilon_{m_2 \sigma}^{\text{QP}})} \right], \end{aligned} \quad (7)$$

respectively. The eigenvector of the BSE  $A_{n\sigma, m\sigma}^\lambda$  and the QP wave function  $\phi_{n\sigma}^{\text{QP}}(\mathbf{r})$  constitute the exciton wave functions as

$$\chi_{\sigma, \sigma'}^\lambda(\mathbf{r}_1, \mathbf{r}_2) = \sum_n^{\text{occ}} \sum_m^{\text{emp}} A_{n\sigma, m\sigma}^\lambda \phi_{n\sigma}^{\text{QP}}(\mathbf{r}_2)\phi_{m\sigma}^{\text{QP}*}(\mathbf{r}_1) \quad (8)$$

in the TDA. Thus, the BSE eigenvector  $A_{n\sigma, m\sigma}^\lambda$  gives the relationship between the QP state and the excitonic state.

The fluorescence photon emission spectra of XES are given by the imaginary part of the macroscopic dielectric function  $\varepsilon_M$  [31]. In the TDA, the macroscopic dielectric function is calculated using the following equation:

$$\begin{aligned} \varepsilon_M^{\text{TDA}}(\omega) &= 1 + \lim_{\mathbf{q} \rightarrow 0} v(\mathbf{q}) \\ &\times \sum_\lambda \frac{\left| \sum_\sigma \sum_n^{\text{occ}} \sum_m^{\text{emp}} \langle n\sigma | e^{-i\mathbf{q}\cdot\mathbf{r}} | m\sigma \rangle A_{n\sigma, m\sigma}^\lambda \right|^2}{\Omega_\lambda - \omega}. \end{aligned} \quad (9)$$

### III. COMPUTATIONAL DETAILS

In this section we will describe computational details for the XES simulation in the *GW* + BSE method. In this paper, we use the all-electron mixed basis program, TOMBO, in which both plane waves (PWs) and numerical atomic orbitals (AOs) are used as basis functions [49]. We select CH<sub>4</sub>, NH<sub>3</sub>, H<sub>2</sub>O, and CH<sub>3</sub>OH molecules as target systems. Besley and

The BSE of Eq. (3) may be regarded as a variant of the Dyson equation for the two-particle Green's function. In the formulation of Eq. (3), the BSE has the electron-electron, the hole-hole, and the electron-hole channels. The BSE of the electron-hole channel is transformed into an eigenvalue problem as discussed by Strinati [29]. In the case of the *GWA* and the TDA, the resulting BSE Hamiltonian for spin-polarized systems is represented as the  $2 \times 2$  block matrix of the  $\uparrow\uparrow - \downarrow\downarrow$  subspace:

$$\begin{pmatrix} D_{\uparrow\uparrow} + X_{\uparrow\uparrow} & X_{\uparrow\downarrow} \\ X_{\uparrow\downarrow} & D_{\downarrow\downarrow} + X_{\downarrow\downarrow} \end{pmatrix} \cdot \begin{pmatrix} A_{\uparrow\uparrow}^\lambda \\ A_{\downarrow\downarrow}^\lambda \end{pmatrix} = \Omega^\lambda \begin{pmatrix} A_{\uparrow\uparrow}^\lambda \\ A_{\downarrow\downarrow}^\lambda \end{pmatrix}, \quad (5)$$

where  $\Omega^\lambda$ ,  $D$ , and  $X$  mean the transition energy of the excitonic state  $\lambda$ , the direct term, and the exchange term, respectively. The direct and exchange terms of the BSE Hamiltonian are given by

$$\begin{aligned} X_{n_1, m_1; n_2, m_2}^{\sigma, \sigma'} &= \int \phi_{n_1 \sigma}^{\text{QP}*}(\mathbf{r}_1)\phi_{m_1 \sigma}^{\text{QP}}(\mathbf{r}_1)v(\mathbf{r}_1 - \mathbf{r}_2) \\ &\times \phi_{n_2 \sigma'}^{\text{QP}}(\mathbf{r}_2)\phi_{m_2 \sigma'}^{\text{QP}*}(\mathbf{r}_2)d\mathbf{r}_1 d\mathbf{r}_2 \end{aligned} \quad (6)$$

and

Asmurf [9] already calculated the XES spectra for these molecules using other *ab initio* methods, e.g., TD-DFT, EOM-CCSD, and  $\Delta$ SCF(B3LYP) methods. These target molecules have also experimental XES data in previous studies [55–58]. We take the input coordinates of these target molecules from the PUBCHEM3D data [53].

Since the initial state of XES is excited, we set the electronic configuration as  $N - 1$  electrons with a core hole. Our calculation procedure is as follows. First, we perform the DFT-SCF calculation of the spin-polarized  $N - 1$  system and determine the KS eigenvalues and wave functions, which include the screening effect induced by a core hole. Second, using the resulting KS eigenvalues and wave functions, we calculate the QP energies using the one-shot *GW* method. Finally, the BSE is solved within the TDA.

All our *GW* + BSE calculations begin with the DFT calculation in the local-density approximation (LDA). We use Perdew-Zunger's exchange-correlation functional [54] for the DFT-SCF calculation. Furthermore, all our calculations include semirelativistic effects (mass-velocity and Darwin terms) in the LDA level for the sake of highly accurate calculations. In the one-shot *GW* and the BSE calculations, the generalized plasmon pole model (GPP) is applied to the dynamical screened Coulomb interaction in the correlation term of the *GW* self-energy [51] and the direct term of the BSE Hamiltonian [28]. As shown in Eq. (7), the matrix element of the BSE direct term  $D$  depends on the transition energy  $\Omega_\lambda$ . In order to treat this dependency, it is required to solve the BSE iteratively in the same way as in Ref. [28].

TABLE I. Molecules, cell parameters (simple cubic), atomic orbitals (AOs), cutoff energies for plane waves  $E_{\text{PW}}^{\text{cutoff}}$ , exchange  $E_x^{\text{cutoff}}$  and correlation  $E_c^{\text{cutoff}}$ , and the number of levels used in the GW+BSE calculations.

Molecule	Cell parameter (Å)	AO	$E_{\text{PW}}^{\text{cutoff}}$ (Ry)	$E_x^{\text{cutoff}}$ exchange (Ry)	$E_c^{\text{cutoff}}$ correlation (Ry)	Number of levels
CH <sub>4</sub>	$a = b = c = 12.0$	C1s	30.7	155.5	17.3	2000
NH <sub>3</sub>	$a = b = c = 10.0$	N1s	69.1	276.4	24.9	2000
H <sub>2</sub> O	$a = b = c = 10.0$	O1s	63.7	276.4	24.9	2500
CH <sub>3</sub> OH	$a = b = c = 14.0$	(C,O)1s	47.4	124.6	18.3	3000

Computational conditions such as cell parameters, AOs, cutoff energies for PWs, the Fock term of the GWA  $\Sigma_x$ , the correlation term of the GWA  $\Sigma_c$ , and the number of levels for target molecules are listed in Table I. All calculations in this paper used periodic boundary conditions. Thus, in order to treat the isolated systems, we used the spherical cut approach for the Coulombic interactions [28].

#### IV. RESULTS AND DISCUSSION

Here, we will show the calculated GW + BSE results and compare them with the preexisting XES data.

##### A. X-ray fluorescence photon energy

Table II lists both experimental and calculated XES fluorescence photon energies of molecular systems CH<sub>4</sub>, NH<sub>3</sub>, H<sub>2</sub>O, and CH<sub>3</sub>OH. Figure 2 shows both experimental and calculated XES spectra of these molecular systems.

CH<sub>4</sub> has one peak in the carbon K-edge spectrum of XES, where the calculated photon energy is 278.3 eV. Comparing with the corresponding experimental photon energy 276.3 eV, the deviation is 2.0 eV for CH<sub>4</sub>. Our GW + BSE result of NH<sub>3</sub> has two peaks at 391.1 and 396.7 eV in the nitrogen K-edge spectrum of XES. There are corresponding

experimental photon energies at 388.8 and 395.1 eV. The deviations between our GW + BSE results and the experimental data are 2.3 and 1.6 eV for NH<sub>3</sub>. Our GW + BSE result for the H<sub>2</sub>O molecule has three peaks at 523.0, 526.8, and 529.2 eV. The corresponding experimental photon energies are 521.0, 525.1, and 527.0 eV. The deviations of the GW + BSE result from experimental data are 2.0, 1.7, and 2.2 eV. For CH<sub>3</sub>OH, our calculated photon energies are 275.7, 278.2, 279.0, 280.8, and 281.4 eV, while the corresponding experimental data are 274.8, 276.6, 277.4, 279.5, and 281.2 eV. The deviations between our GW + BSE results and the experimental data are 0.9, 1.6, 1.6, 1.3, and 0.2 eV for CH<sub>3</sub>OH.

Although there is an overestimation of about 1 eV, the GW + BSE results give fairly good agreements with the corresponding experimental photon energies. Concerning CH<sub>3</sub>OH, the mean absolute error (MAE) of the calculated GW + BSE results is 1.1 eV, whereas the MAEs of preexisting TD-DFT data are 10.4, 6.5, and 1.7 eV for BLYP, B3LYP, and short-range corrected (SRC) [59] exchange-correlation functionals, respectively. The MAEs of the preexisting EOM-CCSD and  $\Delta$ SCF(B3LYP) results are 0.9 and 0.8 eV, although two peaks are missing in all these preexisting results for CH<sub>3</sub>OH. In terms of the accuracy of XES fluorescence photon energies, our GW + BSE method clearly outperforms the

TABLE II. Computed x-ray fluorescence photon energies using the GW+BSE with the TDA (in eV) and preexisting TD-DFT, EOM-CCSD, and  $\Delta$ SCF results and experimental data.

Molecule	Experimental assignment	GW+BSE	TD-DFT <sup>a</sup>			EOM-CCSD <sup>a</sup>	$\Delta$ SCF <sup>a</sup> (B3LYP)	Expt.
			(BLYP)	(B3LYP)	(Short-range corrected)			
CH <sub>4</sub>	$1t_2 \rightarrow 1a_1$	278.3	286.4	283.3	279.5	276.2	276.8	276.3 <sup>b</sup>
NH <sub>3</sub>	$1e \rightarrow 1a_1$	391.1	399.5	395.8	390.8	388.0	388.2	388.8 <sup>c</sup>
	$2a_1 \rightarrow 1a_1$	396.7	406.3	403.0	399.0	395.6	395.3	395.1 <sup>c</sup>
H <sub>2</sub> O	$1b_2 \rightarrow 1a_1$	523.0	534.3	530.0	524.0	521.0	520.9	521.0 <sup>d</sup>
	$3a_1 \rightarrow 1a_1$	526.8	538.2	534.3	528.9	525.4	525.0	525.1 <sup>d</sup>
	$2a_1 \rightarrow 1a_1$	529.2	540.0	536.2	531.3	527.8	527.2	527.0 <sup>d</sup>
CH <sub>3</sub> OH	$5a' \rightarrow 2a'$	275.7						274.8 <sup>e</sup>
	$1a'' \rightarrow 2a'$	278.2						276.6 <sup>e</sup>
	$6a' \rightarrow 2a'$	279.0	287.5	284.1	279.8	276.6	278.0	277.4 <sup>e</sup>
	$7a' \rightarrow 2a'$	280.8	290.1	286.1	281.5	278.7	280.4	279.5 <sup>e</sup>
	$2a'' \rightarrow 2a'$	281.4	291.7	287.4	282.0	280.0	282.0	281.2 <sup>e</sup>

<sup>a</sup>Ref. [9].

<sup>b</sup>Ref. [55].

<sup>c</sup>Ref. [56].

<sup>d</sup>Ref. [57].

<sup>e</sup>Ref. [58].

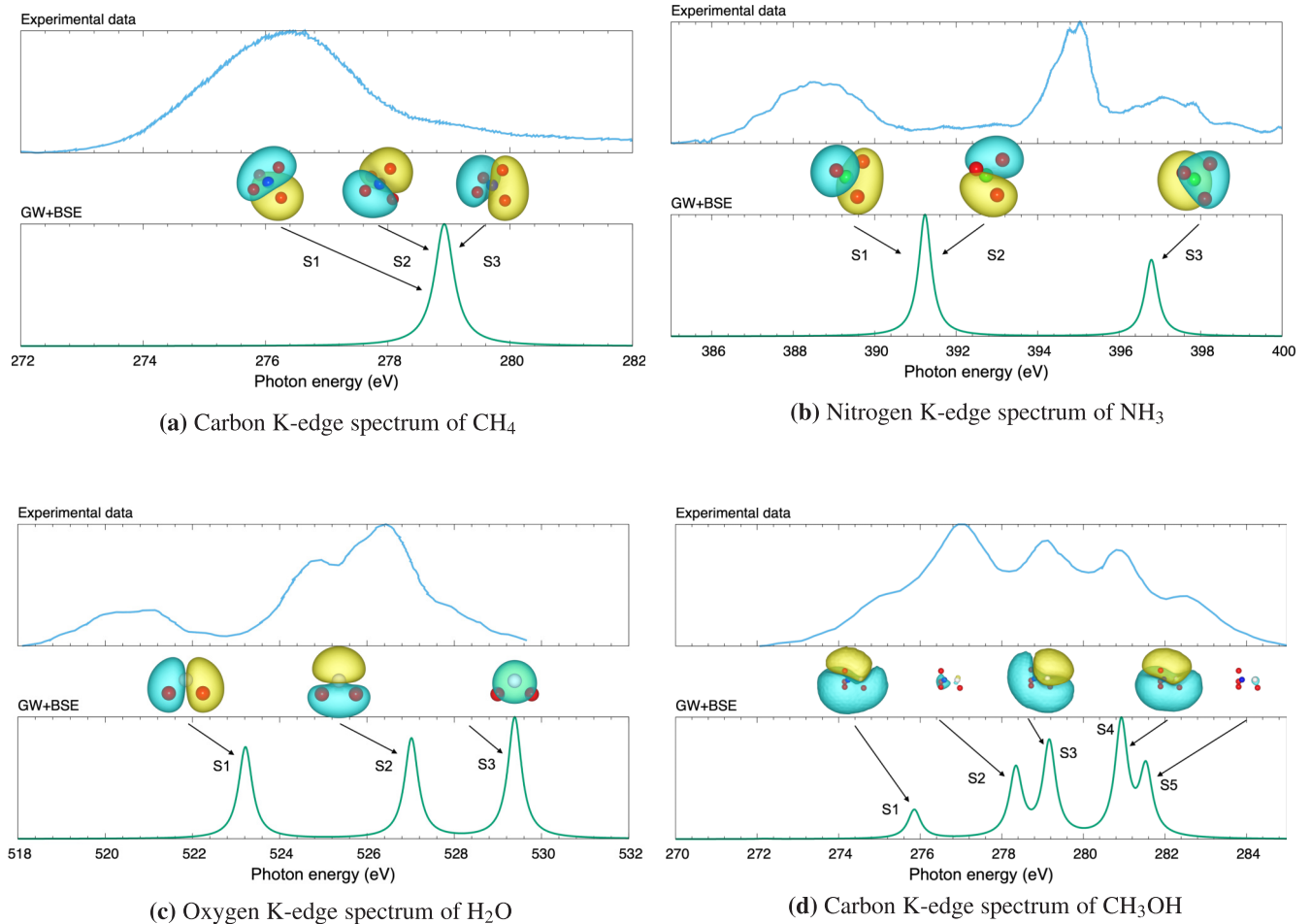


FIG. 2. The experimental and calculated XES spectra of  $\text{CH}_4$ ,  $\text{NH}_3$ ,  $\text{H}_2\text{O}$ , and  $\text{CH}_3\text{OH}$  molecules and the BSE wave functions calculated by the GW + BSE method. The experimental spectra are cited from Refs. [55–58].

TD-DFT method with BLYP and B3LYP functions. Moreover, the accuracy of the GW + BSE method is comparable to the EOM-CCSD and  $\Delta\text{SCF}$ (B3LYP) methods for the purpose of predicting the XES photofluorescence energies.

### B. Spectral assignment

In what follows, we discuss the excitonic effect and the structure of the BSE wave function in the case of XES spectra. We show the calculated and experimental XES spectra with the BSE wave functions in Fig. 2, and the QP energy diagrams with the QP wave functions in Fig. 3. In Figs. 2 and 3, the QP wave functions are real and plotted both positive and negative values. These BSE wave functions are calculated by using Eq. (8), in which the hole position  $\mathbf{r}_h$  is fixed at the center position of an excited atom. In order to understand the assignment of excitonic states, we investigated the relation between the QP wave functions and the BSE wave functions. The GW + BSE method solves the eigenvalues  $\Omega_\lambda$  and the eigenvectors  $A_{vc}^\lambda$  of the BSE Hamiltonian. The eigenvalues and eigenvectors correspond to the exciton excitation (deexcitation) energies and the amplitude for the exciton transition probabilities. Thus, for each XES deexcitation energy  $\Omega_\lambda = \Omega_{S_n}$ , we can obtain the corresponding exciton transition

probability from each valence electron state  $\phi_v(\mathbf{r}_e)$  to the  $1s$  core-hole state of an excited atom  $\phi_{1s}(\mathbf{r}_h)$  as  $|A_{v,1s}^{S_n}|^2$ . Table III shows the valence electron contributions to each excitonic state  $S_n$  in XES spectra. The sum of  $|A_{v,1s}^{S_n}|^2$  over the valence electron states is unity in every excitonic state. That is, each valence contribution  $|A_{v,1s}^{S_n}|^2$  means the ratio of the state hybridization in the excitonic state  $S_n$ .

Figure 2(d) shows the carbon K-edge XES spectrum of  $\text{CH}_3\text{OH}$ . Both the preexisting experimental and present calculated spectra have five peaks. We labeled the five peaks as  $S_n$  ( $n = 1-5$ ), where  $S_1$ ,  $S_2$ ,  $S_3$ ,  $S_4$ , and  $S_5$  correspond to the deexcitation energies of the GW + BSE results at 275.7, 278.2, 279.0, 280.8, and 281.4 eV, respectively. In Fig. 2(d), we also show the BSE wave functions corresponding to each peak  $S_n$ . The excitonic state  $S_1$  at 275.7 eV has the valence electron contributions 64.8, 29.6, 4.3, and 1.3% from HOMO-4, HOMO-1, HOMO-5, and HOMO-2, respectively. We neglected some levels the contributions of which are less than 1%. The excitonic state  $S_2$  at 278.2 eV has the valence electron contributions 73.7 and 26.2% from HOMO-3 and HOMO, respectively. Since both of these orbitals are antisymmetric around the carbon atom, there is no visible amplitude in the BSE wave function for  $S_2$ . The excitonic state  $S_3$  at 279.0 eV has the valence electron contributions 71.0, 23.1, 2.7, and

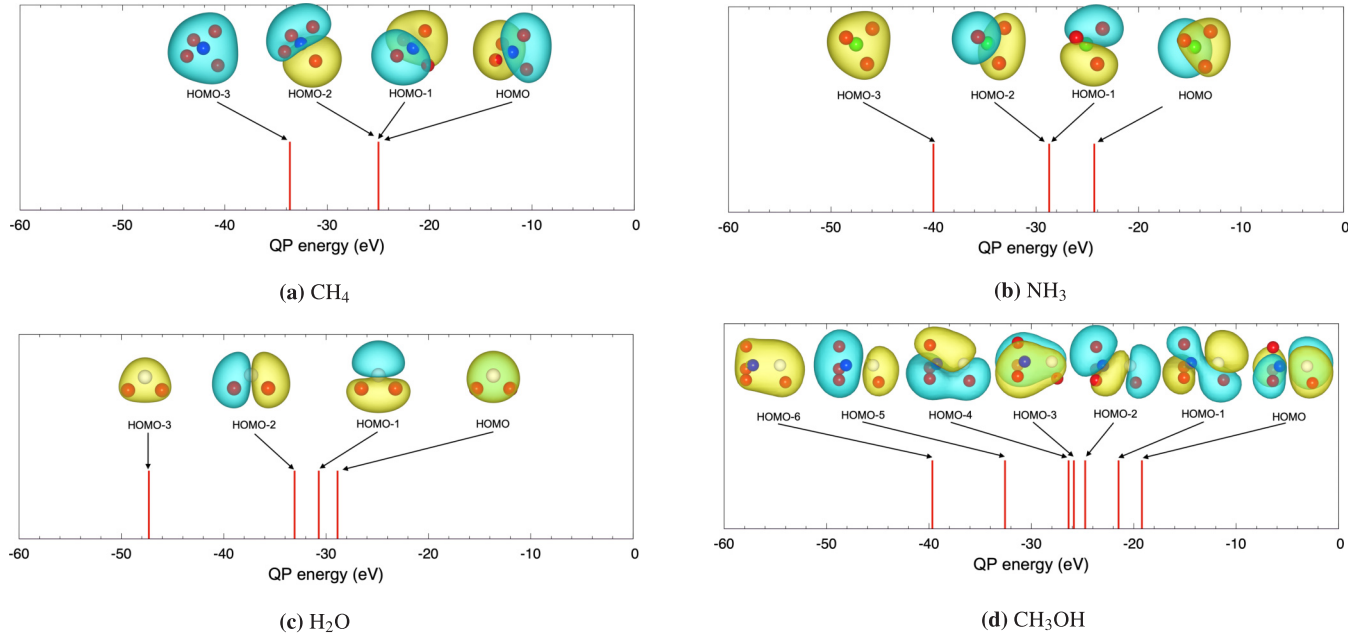


FIG. 3. The calculated QP energy diagrams and the QP wave functions of valence electrons.

2.4% from HOMO-2, HOMO-1, HOMO-4, and HOMO-5 states, respectively. The excitonic state  $S_4$  at 280.8 eV has more than 1% contributions 46.8, 28.9, and 24.2% from HOMO-1, HOMO-4, and HOMO-2 states, respectively. In this state, also, these orbitals are antisymmetric around the carbon atom, and no amplitude is seen in the BSE wave functions. The excitonic state  $S_5$  at 281.4 eV has more than 1% contributions 73.7 and 26.2% from HOMO and HOMO-3 states, respectively. The excitonic states  $S_1$ ,  $S_2$ ,  $S_3$ ,  $S_4$ , and  $S_5$  have the largest contribution from HOMO-4, HOMO-3, HOMO-2, HOMO-1, and HOMO states, respectively. From these results, the obtained excitonic states align in the same order as the QP eigenstates with respect to the excitation energies. However, the state hybridization affects the relative peak position of excitons in the XES spectrum.

In Fig. 2(d), five excitonic states can be classified into two types, i.e., nonsymmetric type and antisymmetric type.  $S_2$  and  $S_5$  excitonic states are the antisymmetric-type excitons. From the above analysis of the valence electron contributions, the QP wave functions of HOMO and HOMO-3 states make the main contributions to the antisymmetric-type excitons. Both HOMO and HOMO-3 wave functions are antisymmetric with respect to a plane containing carbon, oxygen, and hydrogen atoms. There are only two antisymmetric-type excitons because of the combination of two QP wave functions. On the other hand,  $S_1$ ,  $S_3$ , and  $S_4$  excitonic states are the nonsymmetric-type excitons. The QP wave functions of HOMO-1, HOMO-2, HOMO-4, HOMO-5, and HOMO-6 states have no symmetry in the  $\text{CH}_3\text{OH}$  molecule. In these five excitonic states, HOMO-6 and HOMO-5 states do not

 TABLE III. Valence electron contributions  $|A_{vc}^{S_n}|^2$  to each excitonic state  $S_n$ .

Molecule	Excitonic state	$\Omega^{S_n}$	$ A_{vc}^{S_n} ^2$						Total	
			HOMO-6	HOMO-5	HOMO-4	HOMO-3	HOMO-2	HOMO-1		HOMO
CH <sub>4</sub>	$S_1$	278.3				0.0	0.938	0.0211	0.0412	1
	$S_2$	278.3				0.0	0.0438	0.888	0.681	1
	$S_3$	278.3				0.0	0.249	0.00548	0.746	1
NH <sub>3</sub>	$S_1$	391.1				0.0	0.996	0.00431	0.0	1
	$S_2$	391.1				0.0	0.00166	0.998	0.0	1
	$S_3$	396.7				0.000788	0.0	0.0	0.999	1
H <sub>2</sub> O	$S_1$	522.8				0.0	0.999	0.0	0.0	1
	$S_2$	526.6				0.00355	0.0	0.996	0.0	1
	$S_3$	528.9				0.0	0.0	0.0	0.999	1
CH <sub>3</sub> OH	$S_1$	275.7	0.0	0.0428	0.648	0.0	0.0132	0.296	0.0	1
	$S_2$	278.2	0.0	0.0	0.0	0.737	0.0	0.0	0.262	1
	$S_3$	279.0	0.00737	0.0238	0.0272	0.0	0.710	0.231	0.0	1
	$S_4$	280.8	0.000117	0.000371	0.289	0.0	0.242	0.468	0.0	1
	$S_5$	281.4	0.0	0.0	0.0	0.262	0.0	0.0	0.737	1

TABLE IV. The BSE transition energies  $\Omega^{S_n}$ , the QP energy differences ( $\epsilon_{\text{core}} - \epsilon_{\text{valence}}$ ), and the excitonic energy contribution  $\Omega^{S_n} - (\epsilon_{\text{core}} - \epsilon_{\text{valence}})$  (in eV) for each of the XES spectra calculated by the GW+BSE method.

Molecule	assignment	BSE transition energies	QP energy differences	Excitonic contributions
CH <sub>4</sub>	$S_1(\text{C}1s \rightarrow \text{HOMO} - 2)$	278.3	263.3	15.0
	$S_2(\text{C}1s \rightarrow \text{HOMO} - 1)$	278.3	263.3	15.0
	$S_3(\text{C}1s \rightarrow \text{HOMO})$	278.3	263.3	15.0
NH <sub>3</sub>	$S_1(\text{N}1s \rightarrow \text{HOMO} - 2)$	391.1	374.0	17.1
	$S_2(\text{N}1s \rightarrow \text{HOMO} - 1)$	391.1	374.0	17.1
	$S_3(\text{N}1s \rightarrow \text{HOMO})$	396.7	378.4	18.3
H <sub>2</sub> O	$S_1(\text{O}1s \rightarrow \text{HOMO} - 2)$	523.0	502.1	20.4
	$S_2(\text{O}1s \rightarrow \text{HOMO} - 1)$	526.8	504.5	22.4
	$S_3(\text{O}1s \rightarrow \text{HOMO})$	529.2	506.3	22.9
CH <sub>3</sub> OH	$S_1(\text{C}1s \rightarrow \text{HOMO} - 4)$	275.7	264.2	11.5
	$S_2(\text{C}1s \rightarrow \text{HOMO} - 3)$	278.2	264.7	13.5
	$S_3(\text{C}1s \rightarrow \text{HOMO} - 2)$	279.0	265.8	13.2
	$S_4(\text{C}1s \rightarrow \text{HOMO} - 1)$	280.8	269.0	11.8
	$S_5(\text{C}1s \rightarrow \text{HOMO})$	281.4	271.3	10.1

make a large contribution to these excitonic states, since these are forbidden transitions. Therefore, the remaining QP wave functions of HOMO-1, HOMO-2, and HOMO-4 states make the main contributions to the nonsymmetric-type excitons, respectively. In the previous study [9], the carbon K-edge spectrum of CH<sub>3</sub>OH has only three peaks in the results of both TD-DFT(B3LYP) and EOM-CCSD. It is difficult to interpret the spectral assignment from such results. On the other hand, our GW + BSE results clearly exhibited five peaks in the XES spectrum, which agrees with the experimental data [58]. From these results the GW + BSE has the capability to predict and interpret the XES spectra more accurately than TD-DFT and EOM-CCSD approaches.

In Figs. 2(a), 2(b) and 2(c), we show the K-edge XES spectrum and the BSE wave functions of CH<sub>4</sub>, NH<sub>3</sub>, and H<sub>2</sub>O molecules. Although CH<sub>4</sub>, NH<sub>3</sub>, and H<sub>2</sub>O have 1, 2, and 3 peaks, respectively, as shown in Figs. 2(a), 2(b) and 2(c), these molecules have three excitonic states in common. We called each excitonic state as  $S_n$  ( $n = 1-3$ ) in the same manner as the CH<sub>3</sub>OH case. In Fig. 2(a), the XES spectrum of CH<sub>4</sub> has threefold degenerate excitonic states at 278.3 eV. These degenerate excitonic states are originated from the valence electron states of CH<sub>4</sub>. As shown in Fig. 3(a), it can be confirmed that there are triply degenerate QP energy levels at -24.9 eV. We also listed the valence electron contribution to the excitonic states  $S_1$ ,  $S_2$ , and  $S_3$  at 278.3 eV in Table III. The main valence electron contributions to the  $S_1$ ,  $S_2$ , and  $S_3$  excitonic states are 88.8% from HOMO-1, 93.8% from HOMO-2, and 74.6% from HOMO, respectively.

The excitonic states of XES spectra for NH<sub>3</sub> and H<sub>2</sub>O molecules can be interpreted in the same way as in the above discussion. In Fig. 2(b), the XES spectrum of the NH<sub>3</sub> molecule has  $S_1$  and  $S_2$  excitonic states degenerate at 391.1 eV and the  $S_3$  excitonic state at 396.7 eV. For this NH<sub>3</sub> case, the main valence electron contributions to the  $S_1$ ,  $S_2$ , and  $S_3$  excitonic states are 99.6% from HOMO-2, 99.8% from HOMO-1, and 99.9% from HOMO, respectively. On the other hand, the XES spectrum of H<sub>2</sub>O in Fig. 2(c) has the  $S_1$ ,  $S_2$ , and  $S_3$  excitonic states at 523.0, 526.8, and 529.2 eV, respectively. From Table III, the main valence electron contributions to

the  $S_1$ ,  $S_2$ , and  $S_3$  excitonic states are 99.9% from HOMO-2, 99.6% from HOMO-1, and 99.9% from HOMO, respectively. The BSE eigenstates of H<sub>2</sub>O and NH<sub>3</sub> are almost equal to the QP states. This is due to the energy splitting and the different symmetries. In H<sub>2</sub>O, for example, there are only three valence electrons which can refill a core orbital and the symmetries of all these three states are different. Thus, the BSE eigenstates of H<sub>2</sub>O and NH<sub>3</sub> strongly reflect the QP states. In this way, the eigenvector of BSE for each peak gives obvious interpretation concerning the relation between excitonic state and valence state.

### C. Excitonic effect

Finally, we will discuss the excitonic effect on the x-ray fluorescence photon energies in the XES process. Table IV lists the BSE transition energies and the QP energy differences which were previously assigned for each peak in the XES spectra of Figs. 2 and 3. The BSE transition energies  $\Omega^{S_n}$  of XES photoprocesses include the excitonic effect between the core hole state and the valence electron state, whereas the QP energy differences between these states  $\epsilon_{\text{core}}^{\text{QP}} - \epsilon_{\text{valence}}^{\text{QP}}$  do not include the excitonic effect. Therefore, the difference  $\Omega^{S_n} - (\epsilon_{\text{core}}^{\text{QP}} - \epsilon_{\text{valence}}^{\text{QP}})$  means the excitonic contribution to the XES fluorescence photon energy.

The absolute mean values of the excitonic contributions for the carbon K-edge spectra of CH<sub>3</sub>OH, carbon K-edge spectra of CH<sub>4</sub>, oxygen K-edge spectra of H<sub>2</sub>O, and nitrogen K-edge spectra of NH<sub>3</sub> are 12.0, 15.0, 22.0, and 17.5 eV, respectively. Overall results show a tendency for the differences  $\Omega^\lambda - (\epsilon_{\text{core}}^{\text{QP}} - \epsilon_{\text{valence}}^{\text{QP}})$  to be positive. However, in general, the differences  $\Omega^\lambda - (\epsilon_{\text{core}}^{\text{QP}} - \epsilon_{\text{valence}}^{\text{QP}})$  of photoabsorption processes are negative values. This fact can be interpreted as follows.

For photoabsorption processes, the BSE gives excitonic effects which represent binding energies between electron-hole interactions; on the other hand, the BSE excitonic effects in the XES process appear as release energies. Moreover, the initial state in the XES process obtained by the extended quasiparticle method includes the screening effect induced by a core hole at the outset. Therefore this initial state is

already a bound state within the one-shot *GW* approximation. In the XES process, the valence electron decay to refill a core hole relaxes this bound state and releases x-ray fluorescence photon energy.

## V. CONCLUSION

In summary, we developed a method of calculating XES using the *GW* + BSE method. The method enables one to calculate XES all at once in a single calculation. The target systems are CH<sub>4</sub>, NH<sub>3</sub>, H<sub>2</sub>O, and CH<sub>3</sub>OH molecules, which include the chemically important K-edge XES spectra of carbon, nitrogen, and oxygen atoms in the soft-x-ray regime. We found two outcomes in the present paper.

First, our results show that the *GW* + BSE method with the TDA and GPP model gives the fluorescence photon energies of XES with about 1-eV accuracy compared to the experimental data. This accuracy is comparable to the previous results using the TD-DFT with the SRC exchange-correlation functional, EOM-CCSD, and  $\Delta$ SCF results. In terms of the computational scalability, the *GW* + BSE method is advantageous to the EOM-CCSD method. The EOM-CCSD calculation with the localized basis scales as  $N^6$ . On the other hand, the *GW* + BSE calculation using the reciprocal-lattice space representation scales as  $N^4$ . Second, we explored the excitonic structure on XES simulation. We put emphasis on the fact that the calculated *GW* + BSE results reproduce corresponding XES spectra without missing any peak. As an important merit, the *GW* + BSE method can assign excitonic configuration of each peak in XES spectra with the QP levels. This means that the analysis of excitonic structure for each peak gives obvious interpretation concerning the relation between excitonic state and valence state.

Our *GW* + BSE calculation is based on the extended quasiparticle approach, which enables an arbitrary excited

state as an initial state. This property gives the accurate electronic structure for the initial state in the XES process, which includes the screening effect induced by one core hole. From these results showing a good agreement with the preexisting experimental data, we conclude that the present *GE*+BSE method has enough capability to simulate XES spectra.

There is the potential for future work on the topic of *ab initio* XES calculations. There remain slight errors in our calculated results both in the XES transition energies and in the the spectral intensities. We infer these errors from several approximations, such as the plasmon-pole model and one-shot methods. Thus, the full-frequency integration and the self-consistent *GW* calculations will be desirable for more accurate investigations. In order to apply our approach to L-edge XES spectra, spin-orbit coupling is required. For more precise discussion, the vibration effect [60–62] is also important, but this is beyond the scope of the present paper and left for future work.

## ACKNOWLEDGMENTS

This work was supported by a Grant-in-Aid for Scientific Research B (Grant No. 18H01939) from Japan Society for the Promotion of Science. The authors are also indebted to the high performance computing infrastructure (HPCI) social and scientific priority issue “Creation of new functional devices and high-performance materials to support next-generation industries”—to be tackled by using the post-K computer promoted by Ministry of Education, Culture, Sports, Science and Technology—for the use of the supercomputer facilities at the Institute for Solid State Physics at the University of Tokyo, at Hokkaido University, and at the Institute for Materials Research at Tohoku University (Projects No. hp170268, No. hp170190, No. hp180125, and No. hp180220).

- 
- [1] L. Young, K. Ueda, M. Gühr, P. H. Bucksbaum, M. Simon, S. Mukamel, N. Rohringer, K. C. Prince, C. Masciovecchio, M. Meyer, A. Rudenko, D. Rolles, C. Bostedt, M. Fuchs, D. A. Reis, R. Santra, H. Kapteyn, M. Murnane, H. Ibrahim, F. Légaré, M. Vrakking, M. Isinger, D. Kroon, M. Gisselbrecht, A. L’Huillier, H. J. Wörner, and S. R. Leone, *J. Phys. B* **51**, 032003 (2018).
- [2] K. Siegbahn, *J. Electron Spectroscopy and Related Phenomena* **5**, 3 (1974).
- [3] K. Siegbahn, C. Nordling, G. Johansson, J. Hedman, P. F. Heden, K. Hamrin, U. Gelius, T. Bergmark, L. O. Werme, R. Manne, and Y. Baer, *ESCA Applied to Free Molecules* (North-Holland, Amsterdam, 1969).
- [4] F. de Groot, *Chem. Rev.* **101**, 1779 (2001).
- [5] F. de Groot and A. Kotani, *Core Level Spectroscopy of Solids* (CRC, Boca Raton, FL, 2008).
- [6] P. Norman and A. Dreuw, *Chem. Rev.* **118**, 7208 (2018).
- [7] M. W. D. Hanson-Heine, M. W. George, and N. A. Besley, *J. Chem. Phys.* **146**, 094106 (2017).
- [8] J. D. Wadey and N. A. Besley, *J. Chem. Theory Comput.* **10**, 4557 (2014).
- [9] N. A. Besley and F. A. Asmuruf, *Phys. Chem. Chem. Phys.* **12**, 12024 (2010).
- [10] Y. Zhang, S. Mukamel, M. Khalil, and N. Govind, *J. Chem. Theory Comput.* **11**, 5804 (2015).
- [11] I. P. E. Roper and N. A. Besley, *J. Chem. Phys.* **144**, 114104 (2016).
- [12] D. R. Mortensen, G. T. Seidler, J. J. Kas, N. Govind, C. P. Schwartz, S. Pemmaraju, and D. G. Prendergast, *Phys. Rev. B* **96**, 125136 (2017).
- [13] A. E. A. Fouda and N. A. Besley, *Theor. Chem. Acc.* **137**, 6 (2018).
- [14] P. S. Bagus, *Phys. Rev.* **139**, A619 (1965).
- [15] M. P. Ljungberga, J. J. Mortensenb, and L. G. M. Pettersson, *J. Electron Spectrosc. Relat. Phenom.* **184**, 427 (2011).
- [16] H. Ågren and J. Nordgren, *Theor. Chim. Acta* **58**, 111 (1981).
- [17] A. Dreuw and M. Head-Gordon, *Chem. Rev.* **105**, 4009 (2005).
- [18] R. J. Bartlett and M. Musiał, *Rev. Mod. Phys.* **79**, 291 (2007).
- [19] A. D. Becke, *Phys. Rev. A* **38**, 3098 (1988).
- [20] C. Lee, W. Yang, and R. G. Parr, *Phys. Rev. B* **37**, 785 (1988).
- [21] B. Miehlich, A. Savin, H. Stoll, and H. Preuss, *Chem. Phys. Lett.* **157**, 200 (1989).



- [22] A. D. Becke, *J. Chem. Phys.* **98**, 5648 (1993).
- [23] A. D. Becke, *J. Chem. Phys.* **98**, 1372 (1993).
- [24] P. Hohenberg and W. Kohn, *Phys. Rev.* **136**, B864 (1964).
- [25] W. Kohn and L. J. Sham, *Phys. Rev.* **140**, A1133 (1965).
- [26] A. L. Fetter and J. D. Walecka, *Quantum Theory of Many-Particle Systems* (Dover Publications, Inc., Mineola, New York, 2003).
- [27] M. Rohlfing and S. G. Louie, *Phys. Rev. Lett.* **81**, 2312 (1998).
- [28] M. Rohlfing and S. G. Louie, *Phys. Rev. B* **62**, 4927 (2000).
- [29] G. Strinati, *Phys. Rev. B* **29**, 5718 (1984).
- [30] G. Onida, L. Reining, and A. Rubio, *Rev. Mod. Phys.* **74**, 601 (2002).
- [31] S. Albrecht, L. Reining, R. Del Sole, and G. Onida, *Phys. Rev. Lett.* **80**, 4510 (1998).
- [32] G. Csanak, H. S. Taylor, and R. Yaris, *Adv. At. Mol. Phys.* **7**, 287 (1971).
- [33] E. Salpeter and H. Bethe, *Phys. Rev.* **84**, 1232 (1951).
- [34] T. Aoki and K. Ohno, *J. Phys.: Condens. Matter* **30**, 21LT01 (2018).
- [35] M. J. van Setten, R. Costa, F. Vies, and F. Illas, *J. Chem. Theory Comput.* **14**, 877 (2018).
- [36] D. Golze, J. Wilhelm, M. J. van Setten, and P. Rinke, *J. Chem. Theory Comput.* **14**, 4856 (2018).
- [37] Y. Noguchi, M. Hiyama, H. Akiyama, Y. Harada, and N. Koga, *J. Chem. Theory Comput.* **11**, 1668 (2015).
- [38] J. Vinson, J. J. Rehr, J. J. Kas, and E. L. Shirley, *Phys. Rev. B* **83**, 115106 (2011).
- [39] E. L. Shirley, *Phys. Rev. Lett.* **80**, 794 (1998).
- [40] C. Vorwerk, C. Cocchi, and C. Draxl, *Phys. Rev. B* **95**, 155121 (2017).
- [41] L. Hedin and S. Lundqvist, *Solid State Phys.* **23**, 1 (1970).
- [42] L. Hedin, *Phys. Rev.* **139**, A796 (1965).
- [43] F. Aryasetiawan and O. Gunnarsson, *Rep. Prog. Phys.* **61**, 237 (1998).
- [44] L. Hedin, *J. Phys.: Condens. Matter* **11**, R489 (1999).
- [45] K. Ohno, S. Ono, and T. Isobe, *J. Chem. Phys.* **146**, 084108 (2017).
- [46] J. Vinson, T. Jach, W. T. Elam, and J. D. Denlinger, *Phys. Rev. B* **90**, 205207 (2014).
- [47] J. Vinson, T. Jach, M. Müller, R. Unterumsberger, and B. Beckhoff, *Phys. Rev. B* **94**, 035163 (2016).
- [48] E. L. Shirley, J. A. Soininen, G. P. Zhang, J. A. Carlisle, T. A. Callcott, D. L. Ederer, L. J. Terminello, and R. C. C. Pererag, *J. Electron Spectrosc. Relat. Phenom.* **114-116**, 939 (2001).
- [49] S. Ono, Y. Noguchi, R. Sahara, Y. Kawazoe, and K. Ohno, *Comput. Phys. Commun.* **189**, 20 (2015).
- [50] S. M. Dancoff, *Phys. Rev.* **78**, 382 (1950).
- [51] M. S. Hybertsen and S. G. Louie, *Phys. Rev. B* **34**, 5390 (1986).
- [52] W. Kang and M. S. Hybertsen, *Phys. Rev. B* **82**, 085203 (2010).
- [53] E. E. Bolton, J. Chen, S. Kim, L. Han, S. He, W. Shi, V. Simonyan, Y. Sun, P. A. Thiessen, J. Wang, B. Yu, J. Zhang, and S. H. Bryant, *J. Cheminformatics* **3**, 32 (2011).
- [54] J. P. Perdew and A. Zunger, *Phys. Rev. B* **23**, 5048 (1981).
- [55] P. Glans, R. E. La Villa, Y. Luo, H. Ågren, and J. Nordgren, *J. Phys. B* **27**, 3399 (1994).
- [56] J. Nordgren, H. Ågren, L. O. Werme, C. Nordling, and K. Siegbahn, *J. Phys. B* **9**, 295 (1976).
- [57] S. Kashtanov, A. Augustsson, Y. Luo, J. H. Guo, C. Sathe, J. E. Rubensson, H. Siegbahn, J. Nordgren, and H. Ågren, *Phys. Rev. B* **69**, 024201 (2004).
- [58] J. E. Rubensson, N. Wassdahl, R. Brammer, and J. Nordgren, *J. Electron Spectrosc. Relat. Phenom.* **47**, 131 (1988).
- [59] N. A. Besley, M. J. G. Peach, and D. J. Tozer, *Phys. Chem. Chem. Phys.* **11**, 10350 (2009).
- [60] M. Odelius, H. Ogasawara, D. Nordlund, O. Fuchs, L. Weinhardt, F. Maier, E. Umbach, C. Heske, Y. Zubavichus, M. Grunze, J. D. Denlinger, L. G. M. Pettersson, and A. Nilsson, *Phys. Rev. Lett.* **94**, 227401 (2005).
- [61] F. Gel'mukhanov and H. Ågren, *Phys. Rep.* **312**, 87 (1999).
- [62] T. A. Pascal, U. Boesenberg, R. Kostecki, T. J. Richardson, T.-C. Weng, D. Sokaras, D. Nordlund, E. McDermott, A. Moewes, J. Cabana, and D. Prendergast, *J. Chem. Phys.* **140**, 034107 (2014).